UCRL-18437

eg. 2

University of California

Ernest O. Lawrence Radiation Laboratory

THE SUPERCONDUCTING CRITICAL CURRENT AND CRITICAL FIELDS OF Nb_3Sn-NbC AND Nb_3Sn-Nb COMPOSITES

Russell Howard Jones
(M.S. Thesis)

September 1968

Berkeley, California

DISCLAIMER

UCRL-18437

UNIVERSITY OF CALIFORNIA

Lawrence Radiation Laboratory
Berkeley, California

AEC Contract No. W-7405-eng-48

THE SUPERCONDUCTING CRITICAL CURRENT AND CRITICAL FIELDS OF Nb_3Sn-NbC AND Nb_3Sn-Nb COMPOSITES

Russell Howard Jones

(M.S. Thesis)

September 1968

TABLE OF CONTENTS

THE SUPERCONDUCTING CRITICAL CURRENT AND CRITICAL FIELDS OF Nb_3Sn-NbC and Nb_3Sn-Nb COMPOSITES

RUSSELL JONES

Inorganic Materials Research Division, Lawrence Radiation Laboratory, and the Department of Mineral Technology, College of Engineering, University of California, Berkeley, California

ABSTRACT

The critical currents and critical fields of a Type II superconductor are dependent on certain microstructural aspects. These properties have been studied using composite samples with Nb_3Sn surrounding grains of NbC and niobium. Two types of processing treatments have been examined resulting in desirable composite microstructures with good critical current and field values.

Films of Nb_3Sn surrounding NbC grains were obtained by hot pressing powders of niobium, tin, and graphite. Films of Nb_3Sn surrounding niobium grains were obtained with presintered porous niobium impregnated with tin. Metallography, x-ray diffraction and electron beam microprobe were used in the examination of the samples. The critical temperatures were measured and the field properties were determined using the pulsed field technique. The highest critical current (J_{c_N}) obtained was 53,700 amp/cm^2. The highest critical temperature was 17.8°K, and the best upper critical field (H_{c_2}) was 234 kG.

I. INTRODUCTION

The critical fields and critical currents of a Type II superconductor are dependent on certain microstructural aspects. The critical fields are dependent on the average number of electrons per unit volume and the normal state mean free path of the electrons. The upper critical field is also a function of the dimensions of the superconducting phase. The critical currents of the superconductor are affected by the type of pinning sites which are operating.

Previous work by Chabanne[1] with a composite Type II superconductor resulted in an H_{c2} of 240 kG. The composite was NbC grains coated with the high field Type II superconductor Nb_3Sn. The effect of processing temperature upon the critical fields and critical currents of this composite structure were studied in this paper. Also, the effect of the processing technique on the distribution of Nb_3Sn was studied.

Films of Nb_3Sn surrounding NbC grains were obtained by hot pressing powders of niobium, tin and graphite. Films of Nb_3Sn surrounding niobium grains were obtained with presintered porous niobium impregnated with tin.

The resulting microstructures were examined metallographically, and X-ray diffraction was used to identify the phases. The Nb_3Sn composition was determined with the electron beam microprobe. The critical temperatures were measured inductively, and the field properties were measured with pulsed fields. Correlations have been made between critical currents (J) and field (H), the upper critical field (H_{c2}) and critical temperaute (T_c), heat treatment to critical current (J_{cN}) and % Nb_3Sn, and Nb_3Sn composition to critical temperature (T_c).

II. SURVEY OF THEORY

A. Critical Fields

A superconductor in a magnetic field will transform to the normal state when the magnitude of this field reaches a critical value. There is a single critical field for a Type I superconductor and two critical fields for Type II superconductors.

A Type I superconductor in an external field excludes the flux to a field $H = H_c(T)$. A Type II superconductor enters the mixed state at $H_{c1}(T)$ and remains superconducting to $H_{c2}(T)$, as shown in Fig. 1.[2] The penetration of the flux above H_{c1} is favorable when the surface energy of the normal and superconducting phase is negative. This condition is met when $\kappa > 1/\sqrt{2}$ or $\lambda > \xi$. Kappa is a dimensionless parameter which characterizes a superconductor and is equal to λ/ξ. The flux penetrates as a quantum of flux. The flux core of diameter ξ is normal, and the field penetrates the superconducting phase to a distance λ (Fig. 2).[3] The penetration depth (λ) is the depth to which the magnetic field decays to a certain value in the superconducting region.

The upper critical field as given by Gor'kov[4] has the following relationship:

$$H_{c_2} \propto \rho_n \gamma T_c \qquad (1)$$

where: ρ_n = Normal state resistivity.
γ = Coefficient of specific heat.
T_c = Critical temperature.

See Appendix A.

The parameter κ is a function of the mean free path of the electrons in the normal state. Alloying, increased dislocation density and any-

thing that decreases the mean free path (ℓ) will increase κ. With cold working, κ can be made to increase from $<.707$ to $>.707$, and the superconducting behavior will go from Type I to Type II.

The above relation indicates that increased resistivity will increase H_{c_2}. "Cold work usually introduces a statistical distribution of values of H_{c_2} so that a magnetization curve exhibits a tail at higher fields and approaches zero magnetization asymptotically so that measurement of H_{c_2} is difficult."[5]

The value of H_{c_2} has been shown to increase when the size of the superconductor approaches the dimensions of the penetration depth. The following relationships approximately describe the dependence of $H_{c_2}(t)$ with thickness:[6]

for $\ell < d < \xi\ (t)$

$$H_{c_2}(t) \approx (Tc/\ell)^{1/2}\ (1-t)^{1/2}/d \qquad (2)$$

d = thickness of superconductor

$t = T/T_c$

ℓ = mean free path

This equation is valid when $d < \xi(t)$, but when $d < d_c$ there may also be an increase in $H_c(t)$. The following give the relationship for d_c:

$$d_c = \frac{2(5)^{1/2}\lambda}{\kappa(t)} \qquad (3)$$

The critical thickness (d_c) is the thickness below which there is a significant increase in H_{c_2}.[7] The critical thickness (d_c) for Nb_3Sn equals 380°A.*

---

* Obtained from Eq. (3) with $\lambda = 2900$ Å and $\kappa = 34$.

B. Critical Currents

The critcal fields indicate the behavior of the superconductor when there is no transport current. When transport current is present the superconducting transitions are determined by the Lorentz force on the quantized flux. In the mixed state, a Type II can carry current without loss if the quantized flux lines remain in static equilibrium. If the Lorentz force (J×H) is large enough, the flux lines will move. The current density is J and the total magnetic field is H. The movement of the flux lines is said to give rise to the voltage which appears in the mixed state. A Type II superconductor, in the mixed state with J⊥H, and in a field high enough to cause flux movement, will not carry current without loss. The first detectable voltage is termed the J_{c_S}, and J_{c_N} is the transition to the normal state. It has been shown by Kim[8] that the critical current density (J_{c_S}) for Nb_3Sn obeys the following relationship:

$$\alpha = J(H + B_o) \leq \alpha_c \qquad (4)$$

where α_c is a measure of the pinning strength of the material, and $B \approx H_{c_1}$.[9] Dislocations are known to act as pinning sites, as well as a finely dispersed second phases. For a normal second phase it has been shown that J_{c_S} decreases with increasing interparticle spacing (decreasing volume fraction) and increasing particle size (once the particles are large enough to pin several flux threads simultaneously).[10] Flux pinning by magnetic[11] and superconducting[12] precipitates has been demonstrated.

III. EXPERIMENTAL PROCEDURE

A. Sample Preparation

1. Introduction

Two techniques were used for the preparation of samples. One technique is the sintered type and is designated by an S preceding the temperature T_1, as shown in Table I. The term sintering refers to the process of hot pressing mixtures of niobium, tin and graphite. Temperature T_1 is the first holding temperature. The other process utilizes impregnation, and IMP indicates this process. Porous presintered niobium was impregnated with tin. The powders used for all samples are listed in Table II.

2. Sintering Technique

The sintered samples were hot pressed mixtures of niobium, tin and graphite powders. The hot pressing was done in a graphite mold (1-1/4 in. diameter) with a ram type plunger, (1/8 in. × 3/8 in.). The height of the sample was determined by the amount of powder used. The graphite mold was placed on a graphite base, and pressure was applied hydraulically while radiant energy was supplied by a tantalum filament around the graphite mold. Hot pressing was always done under a vacuum (5×10^{-5} mm of Hg) as indicated by an ionization gauge at the main outlet tube.

All temperatures were determined with a Leed's Northrup Optical Pyrometer, with an accuracy of ± 8°C on the high range and ± 14 - ± 25°C on the extra high range. The highest sintering temperatures were 2000°C. Since the extra high range is 1500-2800°C the accuracy at 2000°C was estimated to be ± 20°C. The temperatures were obtained by viewing

through a quartz window and sighting on a horizontal surface of the mold. This does not give the actual temperature of the sample but rather a relative one. A thermocouple was used to determine the temperature of the sample for comparison with the optical pyrometer reading. As expected, there was a lag in the sample temperature on heating because of the time needed to conduct through the graphite mold. For the calibration, the sample temperature was allowed to stabilize before readings were made. It was found that up to 1100°C there was little difference in the temperatures after stabilization, but at 1600°C there was about 100°C difference, with the surface reading being low. These temperature differences resulted when the sample temperature was allowed to stabilize. When continuous heating was used, and time at temperature was short, then there was a lag due to temperature gradients in the mold. Equal rates of heating were used and equal times at temperature, so comparison between heat treatments could be made.

The starting mixture of the sintered series was 1:.56:.66 Nb-Sn-C atom ratios. Sample S1900 S had tantalum added and it had a 1:.56:66:33 Nb-Sn-C-Ta atom ratio. The particular atom ratios were established by Chabanne.[1] The amount of Sn used was more than needed to form a network of Nb_3Sn because tin was lost by evaporation and mold leakage. The powders for the sintered samples were mixed thoroughly by rolling. The graphite was a finer mesh than tin and niobium so care was taken to insure the best possible mixing of graphite.

The heating cycle for the sintered series was as follows: a load of 8000 psi was applied and then the sample was heated directly to the temperature desired. The samples were cooled in a vacuum to the annealing temperature. The 8000 psi load was removed after the annealing

treatment. The heating cycle was varied for samples S1050 and S500. A schematic of the heating cycles is shown in Fig. 3a and 3b.

The primary processing variables were the sintering temperature and the annealing time. For the Type A the sintering temperature varied from 1600°C to 2030°C, and the sintering time was always 8 min. The annealing temperature was always 1100°C and the time was either 15 min.(S) or 60 min. (L). The sintering pressure remained constant at 8000 psi.

The processing treatment (Type B) was to achieve a better distribution of Nb_3Sn. The temperature T_1 was selected to allow the tin to coat the niobium grains prior to compaction at a higher temperature. A low pressure was applied so the liquid tin would not be squeezed out. The annealing treatment was not used in this series.

3. Impregnating Technique

The porous niobium for the impregnating technique was obtained by screening -325 mesh powder through a -200 mesh screen, and the powder which remained was used. This powder was loaded into a mold and hot pressed at 1400°C for 30 min. with a pressure of 1000 psi. The porous niobium was impregnated with tin in a later treatment. The tin was loaded into the mold along with the porous niobium and heated as shown in Fig. 3C. The molds and hot pressing techniques were the same as outlined for the sintered type.

Sample IMP1 was heated to approximately 800°C to allow the tin to fill the porous niobium. Two minutes at 1050°C were allowed for the reaction of tin and niobium. The plan for this series was for the tin to fill the porous niobium without reaction to Nb_3Sn. A subsequent treatment would determine the thickness of Nb_3Sn film. A difficulty

encountered was that, tin would not wet the niobium at a temperature low enough to sufficiently reduce the niobium - tin reaction.

B. Sample Testing

The critical superconducting temperatures were determined inductively and the transition temperatures were measured with a calibrated germanium resistor. The values recorded in Table I are accurate to 0.1°K. For further disucssion on the critical temperatures see M.S. thesis by Roger Goolsby.[13]

The goal of this work was the study of the relationship of the field properties and structure of these samples. Measurements were made using the pulsed field technique, and a schematic of the equipment is shown in Fig. 4. The samples were mounted onto a probe which used the standard four connection resistivity arrangement. The sample was immersed in a cryostat containing liquid helium. The cryostat had a special finger to go inside the inner diameter of the coil. To facilitate cooling, the coil was immersed in liquid nitrogen. The samples were spark cut to a cross section of $10\text{-}20 \times 10^{-3} cm^2$. The ends of the samples were copper plated to allow soldering the samples to the current leads. The voltage leads were held against the samples by pressure. The sample, sample holder and coil assembly were made as rigid as possible to minimize electrical noise.

The direct transport current was initiated prior to the magnetic pulse. Then the transport current was shut off at the peak field, as shown in Fig. 5. This was done to reduce heating. The change of sample voltage with magnetic field was followed with a dual beam oscilloscope and records were taken with high speed polaroid film.

With the sample current zero the voltage induced in the wiring by the magnet field was recorded on the same picture. The voltage curve without transport current was then subtracted from the voltage curve with transport current; the result is the voltage change of the sample.

The magnet rise time was about 10 msec and the maximum field available was about 220 kG. At the high fields the coil was allowed to cool between pulses for 15-20 min. The cooling was to keep the coil from failing and also to reproduce the field between recording the noise and the actual test.

The oscilloscope used was a Tektronic dual beam with type 21-22 time base units. Type D and E amplifiers were used for the field and sample voltage respectively. A type 55 power supply was used. The frequency response for the sample voltage was 10 kc. If too low a frequency response was used rounding of the voltage curve would result, and too large a frequency response would show too much high frequency noise.

Figure 5a shows the polaroid picture of a high field test and Fig. 5b a low field high current density test. Figure 5b shows a sharp transition from superconducting to normal, which means there is little difference between J_{cS} and J_{cN}. Also, Fig. 5b shows that there is little trouble from electrical noise at low values of H. Figure 5a shows a test at a high field with electrical noise present. This noise is recorded by pulsing the coil at the same field as the test but with zero sample current. The difference between the noise and the test voltage is the voltage of interest.

The J_{cS} curve is obtained by plotting the field which produces the first detectable voltage versus the current density. The J_{cN} curve

is obtained by plotting the field at which the voltage ceases to increase against the current density. The resistivity (ρ_n) is obtained from the voltage drop of the normal sample at 4.2°K. The resistivity of the sample at zero field is ρ_2. These values are recorded in Table III. The upper critical field is obtained by extrapolating the J_{c_N} curve to zero current. The extrapolation was a linear extension of the curve. The current density and the field values are accurate to 5%.

Electron beam microprobe analysis was made on samples S1950L, S1730S, S1730L and S500. Because of the multiphase structure there was difficulty distinguishing the phases. The surface was anodized and counts were taken, the anodized coating was removed and counts were again taken. This technique allowed comparison of the counts anodized to counts unanodized, therefore comparison could be made between anodized color and the phase. Care was taken in removing the anodized coating so as not to relieve the surface. Any relief would change the takeoff angle of the characteristic radiation. The composition of Nb_2Sn, in the four samples noted above, was determined with corrections for absorption, background, deadtime and instrument drift. The results were calculated by computer. For the other phases, the counts were taken with the anodized coating present because exact analysis was not necessary.

X-ray diffraction utilizing an X-ray diffractometer was also used to identify the phases present. The samples were mounted in lucite mounts. The tube voltage was 40kV, current 14 ma, ratemeter time constant 3, cps range 200, x-ray source tube target cu, Ni filter, omega 0°, T.O. 4°, slits 1°, 1° and 0.002". Phases other than NbC were not always observed because of their small volume fractions.

Anodizing with Pickelsimer's solution with 27v for 6 min. at room temperature resulted in distinct contrast between phases. The phases observed are listed in Table IV. The samples were prepared by conventional metallographic technique with the last polishing step, on 1μ diamond. Sample IMP 1 presented a problem polishing because of the niobium grains and large volumes of tin. The technique used for IMP 1 required a final polish of 0.3μ alumina, H_2O_2 and NaOH in H_2O.

IV. DISCUSSION OF RESULTS

A. Microstructures

The superconducting critical currents can be related to the microstructures of the composite samples investigated. The amount and distribution of Nb_3Sn and tin is important and were the reasons for the variations made to the processing treatment. Phases other than Nb_3Sn and tin were present in all samples. The phases and their distribution are discussed in the following sections.

1. Sintered Type

a. Type A. The sintered type samples were a mixture of phases in which NbC was usually the matrix and the Nb_3Sn was dispersed around some of the NbC grains. The NbC anodized yellow and was easily identified with x-ray diffraction. Microprobe analysis showed that there was very little tin in the NbC grains. Nb_3Sn anodized as a dark blue or violet color and could be identified by microprobe. Nb_3Sn could not always be identified with x-ray diffraction because the volume fraction was too small. The phase which anodized as dark brown is thought to be Nb_3Sn_2. The composition of the brown phase did not compare exactly with Nb_3Sn_2. However, the microprobe analysis was done with the anodized coating intact and this could account for some of the deviation. A light brown phase which appeared in varying amount was checked for tin and none was found. This phase is shown in Fig. 6b and could possibly be Nb_2C. Niobium anodized as a light blue and it was present in S1703S. Also present in most samples was excess tin and graphite.

The niobium-tin constitution diagram has been studied by many workers. Figure 7 shows the phase diagram proposed by Ellis et al.[14]

The composition of the intermetallics is a matter of disagreement. The phases indicated in Fig. 7 will be used throughout this paper.

All three intermetallics of the niobium-tin system are superconducting. The T_c of Nb_2Sn_3 is 2.4 to 3.4°K and at 2°K the critical field is 200 G.[15] Nb_3Sn_2 has a T_c of less than 2.8°K and its critical field is 600G.[2] Nb_3Sn has a T_c of about 18.0°K and an H_{c_2} of approximately 220 kG at 4.2°K.[16] The current density of Nb_3Sn at 88 kG has been shown to be 10^5 amp/cm^2.[16] Nb_3Sn has the beta tungsten crystal structure and it has been shown to exist over a range of compositions of (Nb_xSn_{1-x}) x = 0.80-0.72X when prepared at 1200°C. The lattice constant is about 5.209Å and ranges from 5.282-5.290 as x goes from 0.80-0.72.[16]

The distribution of the Nb_3Sn is easily seen when the samples are anodized. For the sintered type the amount and distribution of Nb_3Sn was dependent on the maximum sintering temperature, as shown in Table V. Comparing Figs. 6a, 8, 9a, 10a, 11a and 12, the amount of Nb_3Sn can be seen to increase with decreasing sintering temperature. The heating cycle for these samples is given in Table I. For these samples, the amount of Nb_3Sn was dependent on the maximum temperature, because they were heated directly to the upper sintering temperature. The maximum reaction rate for Nb_3Sn is at about 1000°C, and at 1400°C NbC will form in appreciable quantities. The reaction of tin with NbC is negligible, so no Nb_3Sn will form after NbC has formed. Samples S1730L and S1730S indicate the variation possible due to the mold condition.

The sequence of chemical reactions is believed to be as follows. The mixed powders are compressed and heated. The tin melts at 232°C

and will tend to segregate because of the lack of wetting. Upon further temperature rise, the tin reacts with niobium to form Nb_3Sn, resulting in segregated regions of Nb_3Sn. Further temperature increase will result in carbon reacting with niobium to form NbC. Excess carbon was usually found in two regions: 1) with the excess tin and not in solution; 2) surrounded by a group of NbC grains. The carbon in the latter case could diffuse into the niobium and form NbC but in the former case would have to diffuse through Nb_3Sn in order to react with niobium. Upon cooling from the sintering temperature it is thought that further reaction of niobium and tin does not occur. The annealing treatment allowed the excess tin to restore the stoichiometry of the Nb_3Sn phase.

b. Type B. The distribution of Nb_3Sn was greatly changed by allowing time for the tin to react with niobium before NbC formed. Examples of the microstructures are shown in Figs. 13 and 14. Sample S1050 has a large volume of well dispersed Nb_3Sn, but is not a continuous film. Some grains of NbC are coated with a film, but the major proportion of Nb_3Sn is in large globular shapes. The phases present are NbC, Nb_3Sn and Nb_3Sn_2(dark brown phase). This brown phase is distributed the same as Nb_3Sn and quite often breaks up the continuity of the Nb_3Sn. Assuming the dark brown phase is Nb_3Sn_2, it probably formed upon cooling because Nb_3Sn_2 is not stable above 930°C.

The grain size of sample S1050 is quite small compared to other samples. The reduction of grain growth is probably due to the coating of Nb_3Sn around each grain. The grain size is very close to the original powder size of the niobium. The niobium powder size is -325 mesh, and most of the powder will go through a screen opening of 0.0017 in.

Measurement of the grains at 1000x shows that nearly all are smaller than 0.0017 in.

Sample S500 was given a similar treatment to that of S1050 but the temperatures were somewhat lower. The result was a greater percentage of Nb_3Sn in S500 than in S1050. The T_1 temperature was lower than the temperature for maximum Nb_3Sn reaction and also lower than T_1 of S1050. The upper temperature of S500 could account for the greater amount of Nb_3Sn since it is lower than that of S1050. The NbC would form slower thus allowing the tin more time to react with the niobium. The phases which were present were NbC, Nb_3Sn, Nb_3Sn_2 and Nb.

2. Impregnated Type.

The impregnation of porous niobium with tin was used to control the distribution and amount of Nb_3Sn. The method used was outlined earlier, and the result is shown in Fig. 15. However, tin would not penetrate at a temperature low enough to reduce the reaction of tin and niobium. If the tin could fill the niobium compact without reaction, then the amount of Nb_3Sn formed could be controlled.

The phases present in IMP 1 are listed in Table IV. The presence of Nb_3Sn is confirmed by the high T_c, and the matrix anodized blue as niobium does. There was a yellow brown phase of undetermined composition which was more continuous than the Nb_3Sn. Comparison was made of the anodized color with the results of Enstrom et al.[17] The niobium and Nb_3Sn are similar, but the yellow brown does not match anything listed. Since unreacted tin is observable in IMP 1 the yellow brown is not the yellow listed by Enstrom et al. X-ray data give peaks which are common

to both Nb_3Sn_2 and Nb_2Sn_3 phases, so it cannot be concluded which of these two is the yellow brown phase.

B. J-H Relationships

1. Sintered Type.

The J-H curves shown in Fig. 16 are for the Type A sintered samples. The curves shown are J_{c_N} curves in which the sample has changed to the normal state resistivity. The differences in the current densities are discussed in another part of this report. The extrapolation to $J = 0$ gives the value for H_{c_2}. The extrapolation was done as a linear extension of the curve rather than a vertical extrapolation which is the usual shape of the curve. The extrapolated H_{c_2} values are high because of this. A linear extension was used because the vertical drop would have depended on the highest field obtained for that test. In some tests the noise was balanced and compensated for more effectively, thus higher field data could be obtained for some samples.

The difference between the sintering treatment with a plateau (Type B) and without the plateau (Type A) is illustrated in Fig. 17. Since the current density is determined by the cross section of the total sample, increasing the volume fraction of Nb_3Sn should increase the current density of the total sample. The results shown in Table VI do not show this trend because of the effect of the other phases such as tin and Nb_3Sn_2.

The J-H curves shown in the preceding figures show only a J_{c_N} curve. There is no J_{c_S} shown because these samples had a voltage drop for the lowest field measureable. The voltage at low field is attributed to NbC, Nb_2C, Nb_3Sn_2 and tin which are the phases linking the

discontinuous Nb_3Sn. It has been shown that NbC has a J_{c_N} of 10-15 kG at the current densities used in this experiment.[18] The NbC is in the normal state for most of the field pulse of this experiment, so there is a voltage drop due to normal NbC. The heating from the normal NbC could also cause the Nb_3Sn to transform prematurely to the normal state. The results shown in Table VI do not show this trend because of the affect of the other phases such as tin and Nb_3Sn_2. J_{cS} for Nb_3Sn has been determined in a steady field by Montgomery.[19] If the Nb_3 Sn was continuous in these samples similar J_{cS} curves would be expected. At lower and higher current densities the J_{cS} approaches the J_{c_N} so a sharper transition results. This can be seen in Fig. 5b. Fig. 5b illustrates how NbC controls the transition at lower fields. There is little measurable voltage up to a field of about 10 kG above which it is seen that the transition to the normal state occurs over a small range of fields. At low fields and high current densities the properties of these samples reflect the NbC properties more than the properties of Nb_3Sn. The heating from the normal NbC will force the Nb_3Sn to become normal simultaneously with the NbC. At high fields and low current densities the NbC causes some heating, but does not cause the Nb_3Sn to become normal simultaneously with the NbC. The current densities of these samples at high fields is about 1/5 - 1/10 of Nb_3Sn. The volume fraction of Nb_3Sn could account for this.

The resistivity ρ_2 of the sample at H = 0 increases as the amount of Nb_3Sn decreases, as illustrated in Table VI. This is expected because the distance between the superconducting phase increases. Figures 18a and b shows the relationship between the voltage and field for samples S1930S and S1730S. The resistivity ρ_2 represents the voltage difference

between the noise and sample voltage at H = 0. The higher ρ_2 values correspond to the samples with the least amount of Nb_3Sn. Sample S1050 does not completely follow this trend. The distribution of Nb_3Sn accounts for the low ρ_2.

The rise time of the magnetic coil in this experiment is about 10 millisec, and at 200 kG a $dH/dt = 2 \times 10^7$ G/sec results. Flippen[20] found that the resistive transition of Nb_3Sn was lowered to 75 kG at low current densities when dH/dt of 5×10^{10} G/sec. In a steady field at a similar current density the resistive critical field was 200 kG. Hart et al[21] in their study of Nb_3Sn in pulsed fields found a decrease of the critical current with the faster pulse. The slowest coil had a maximum $dH/dt = 1.6 \times 10^7$ G/sec, and the critical current did not vary when this rate was decreased by lowering the maximum field. The faster coil Hart et. al used had a maximum $dH/dt = 6 \times 10^7$. It was found that near the peak field the transition was higher because of the decreased dH/dt. Flippen found that Nb_3Sn in contact with niobium had a resistive critical field of less than 100 kG when there was a 7 kG steady field superimposed to keep the niobium normal. This low critical field is attributed to the normal niobium. The normal niobium could be similar to the effect observed in this work in which the NbC matrix is normal at a very low field. In this work the NbC matrix, rather than the pulse rate, is thought to be responsible for the low J_{cs}.

2. Impregnated Type

The best sintered type sample is compared with the impregnated type sample in Fig. 19. The similarity of the curves is apparent. The impregnated sample has Nb_3Sn surrounding grains of niobium and the

sintered has Nb_3Sn surrounding grains of NbC. The two samples have a similar distribution of Nb_3Sn and both have a good deal of free tin.

The niobium grains of sample IMP1 would be normal for the majority of the field test, as would the NbC grains of S1050. The niobium has a lower resistivity than NbC so less heating would occur in sample IMP1. Less heating would result in a high J_{c_N} curve, but IMP1 has a smaller volume fraction of Nb_3Sn than S1050.

C. H_{c_2} Versus T_c

It was shown in the theoretical section of this paper that the upper critical field varies approximately linearly with T_c. The slope of this relationship is the product $\rho_n\gamma$. The coefficient of specific heat is proportional to N(0), the density of states at the Fermi surface, and T_c is proportional to $\epsilon - \frac{1}{N(0)V}$. As the composition of Nb_3Sn approaches stoichiometry from niobium rich the T_c increases. The increase in critical temperature is due to an increase in γ.

The extrapolated H_{c_2} values of the sintered type samples are plotted versus T_c in Fig. 20, with a nearly linear relationship resulting. If the equation $H_{c2} \propto \rho_n \gamma T_c$ is used, the linearity is correct if $\rho_n\gamma$ remains constant. Table VII gives the data for these samples.

The product $\rho_n\gamma$ is constant because the coefficient of specific heat (γ) increases as the composition approaches stoichiometry, and the resistivity would be expected to decrease as the composition approaches stoichiometry.

The results for sample S500 and S1900S are not plotted because they deviate from the plotted curve. The data for S500 would fit a line with

a smaller slope. The smaller product ($\rho_n\gamma$) is thought to be due to a low ρ_n. The low resistivity could be because of the 1500°C sintering temperature. The data of S1900S would fit a line with a larger slope. The tantalum added to this sample would lower γ but raise ρ_n. The resistivity must increase more than γ, because the product $\rho_n\gamma$ increases.

The microprobe analysis of the compositions shows that the tin composition decreases as the T_c decreases. This same result has been reported by Bachner[22] where the vacancies resulting from tin loss are filled with niobium atoms. This results in the breaking up of the niobium atom chains in the crystal. In this work the tin loss was restored by annealing at 1100°C when there was free tin available to restore the stoichiometric composition. Comparison of S1950L and S1930S illustrates this. A sintering temperature of 1600°C and a 60 min. anneal resulted in the highest T_c. The upper critical field (H_{c_2}) of samples S1950L, S1730S and S1730L decreases with increasing niobium concentration. This variation is expected because of the relationship of H_{c_2} to T_c.

D. Critical Currents

1. Sintered Type

The effect of sintering temperature of J_{cN} is shown in Table VIII. The results show that the current density of the Type A composite at 120 kG increases with increasing sintering temperature at a constant annealing time. Increased annealing time at an equal sintering temperature decreases the current density. The current densities of the Nb_3Sn phase are separated more than the composite current density because the samples sintered at the higher temperature also have the lower volume fraction of Nb_3Sn. The trend between samples S1930S, S1730S, S1950L, and S1730L

is to have a lower J_{c_N} the lower the sintering temperature or the longer the anneal. This decrease in J_{c_N} does not follow the change in T_c or the Nb_3Sn composition. The J_{c_S} curve is the first measurable voltage and is explained by the movement of flux lines. The pinning force on the flux line is overcome at J_{c_S}. J_{c_N} is a measure of the transition to the normal state and the variation of J_{c_N} with these samples seems to depend on the distribution of phases.

If the volume fraction of Nb_3Sn is accounted for, the current densities of these samples are lower than those reported for Nb_3Sn.[23] Montgomery's samples have current densities at 120 kG of 2 - 7 x 10^4 amp/cm^2. The samples reported in this work have current densities of .66 - 5.4 x 10^4 amp/cm^2. The lower values could be due to heating which results from the normal NbC.

Another factor is the amount of unreacted tin which is present. This tin could carry some of the current without too much loss even though it is in the normal state. This effect can be seen by comparing samples S1050 and S1730S, in which S1730S has the larger volume fraction of Nb_3Sn, but a J_{c_N} of 1/3 that of S1050. S1050 has a large amount of unreacted tin, and this tin may carry current with less heating than the NbC. The unreacted tin could also explain the high J_{c_N} of samples S1930S and S1950L.

The sintering treatment does not seem to affect the J_{c_N} of the composite sample by the resulting Nb_3Sn distribution. Table IX shows there is no correlation between % Nb_3Sn and J_{c_N} of the total sample. The amount of tin which is present is the controlling factor.

2. Impregnated Type

Sample IMP1 had unreacted tin as well as niobium grains. Pure

niobium has a resistivity of about 5μ ohm-cm at 4.2°K compared to about 10μ ohm-cm for Nb_3Sn and 1 μohm-cm for pure tin. The combination of tin and niobium could carry current with less voltage drop than normal Nb_3Sn. The current density of the Nb_3Sn would be decreased when the Nb_3Sn resistivity in the mixed states rises above the resistivity of the Nb-Sn combination.

E. Resistivity

The normal state resistivity is an important parameter of a superconductor, since the mean free path can affect the critical temperature as well as H_{c_2}. The recorded resistivities are for the total sample, and the volume fraction of Nb_3Sn and tin affect it most.

Table VIII lists the resistivity values, and it can be seen that there is no relationship between ρ_n and T_c. T_c will usually decrease with a decrease in mean free path, and the only sample that exhibits this decrease is S1900S. The high ρ_n is accompanied by a low T_c due to the tantalum which was added. Niobium and tantalum are 100% soluble, so some of the tanalum could have replaced some of the niobium in the Nb_3Sn structure. The T_c of 14.8°K would not be that of TaC, because TaC has a T_c of 9-11.4°K[18].

The resistivity at 4.2°K of stoichiometric Nb_3Sn is about 10 μohm-cm[24] and NbC is 35.1 μohm-cm,[18] and pure tin about 1 μohm-cm.[11] The resistivities of the samples are 2 to 3 times above those of NbC and can only be explained by heating effects. The resistivities are calculated from the voltage drop along the sample when it has transformed to the normal state. If heating occurred because of the normal NbC phase, the resistivities would be increased.

The most interesting comparison is that of ρ_n for IMP1 with the sintered type samples. The low resistivity is attributed to the niobium grains and excess tin. Also, the samples with the lowest resistivity ρ_n (S1930S, S1950L, S1050) are those which have the most excess tin. Sample S500 has a low ρ_n because of its large volume fraction of Nb_3Sn. S1050 has a large volume fraction of Nb_3Sn. S1050 has a large volume fraction of Nb_3Sn as well as excess tin.

V. SUMMARY AND CONCLUSIONS

The superconducting properties of composite Type II superconductors have been determined, and the results are similar to the work of others. The sintered samples resulted in grains of NbC coated with Nb_3Sn, and the impregnated samples resulted in niobium grains coated with Nb_3Sn.

A. Sintered Type

The sintered samples were shown to obey the relationship $H_{c_2} \propto \rho_n \gamma T_c$. The best properties obtained are as follows:

1. J_{c_N} = 3000 amp/$_{cm}^2$ (composite)
2. J_{c_N} = 53,700 amp/$_{cm}^2$ (Nb_3Sn only)
3. T_c = 17.8°K sintered at 1600°C
4. H_{c_2} = 234 kG

The critical temperature of 17.8°K corresponded to an Nb_3Sn composition of 75.3 at % Nb.

The critical current (J_{c_N}) was highest when large amounts of tin were present. The critical current (J_{c_N}) did not vary with T_c or Nb_3Sn composition. The low critical current (J_{c_S}) of these samples is attributed to phases which seperate the Nb_3Sn and are not superconducting or have lower field properties.

The percentage of Nb_3Sn in the composite was dependent on the sintering temperature T_1. The higher this temperature the less Nb_3Sn. The distribution of Nb_3Sn was greatly enhanced by lowering T_1 to about 1050°C. The resistivity of these samples is a measure of the composite resistivity and was lowest when excess tin was present.

B. Impregnated Type

The impregnated samples had a good distribution of Nb_3Sn. The properties of this series were:

1. J_{c_N} = 3400 amp/$_{cm}^2$ (composite)
2. T_c = 17.6°K
3. H_{c_2} = 225 kG

The achievement of a thin continuous network of Nb_3Sn is dependent on the tin wetting the niobium powders. This is true for both the sintered and the impregnated samples a suggestion for further work is the addition of a wetting agent to the tin. Both samples S1050 and IMP 1 could be improved with this technique.

The best properties for a sintered sample were: H_{c2} = 230 kG, T_c = 17.2°K and J_{c_N} = 3000 amp/$_{cm}^2$. The properties of the impregnated series were: H_{c_2} = 225 kG, T_c = 17.6°K and J_{c_N} = 3400 amp/$_{cm}^2$.

APPENDIX A

The upper critical field of a Type II superconductor is dependent on κ and H_c. The relationship for H_{c_2} given by Gor'kov[4] is:

$$H_{c_2} = [\ 1.77 - 0.43\ (T/T_c)^2 + 0.07\ (T/T_c)^4\ ]\ \kappa\ H_c = A(t)\kappa H_c$$

$$\kappa = [\ 21\ \zeta\ (3)/2\pi\ ]^{1/2}\ (\ e\rho_n\gamma^{1/2}/\pi^3 k_B)$$

$$H_c = 2.42\ \gamma^{1/2}\ T_c\ [\ 1 - (T/T_c)^2\ ]$$

With substitution for κ and H_c the equation for H_{c_2} is :

$$H_{c_2} = 2.42\ A(t)\ [\ 25/2\pi\ ]^{1/2}\ [\ e/\pi^3 k_B\ ]\ \rho_n\gamma T_c\ [\ 1 - (T/T_c)^2]$$

where:

e = Electronic charge in emu

k_B= Boltzmann's constant

ρ_n= Normal state resistivity

γ = Electronic specific heat coefficient/ unit vol.

T_c= Critical temperature

T = Temperature

The testing conditions for this experiment with $T = 4.2°K$ and $T_c = 16 - 18\ °K$, $(T/T_c)^2$ and $(T/T_c)^4$ have little effect on the relationship for H_{c_2}. The relationship for H_{c_2} can be simplified as follows:

$$H_{c_2} \propto \rho_n\gamma T_c$$

REFERENCES

1. Jean Chabanne, Effect of the Microstructure on the Superconductive Properties of Nb_3Sn in a NbC Matrix, M.S. Thesis, University of California, Berkeley, UCRL-17826, Sept. 1967.
2. T.G. Berlincourt, Type II Superconductivity, Rev. Mod. Phys. 19 (1964).
3. C. Kittel, Superconductivity, in Introduction to Solid State Physics, 3rd edition (John Wiley and Sons, New York, 1967), pg. 369.
4. T.G. Berlincourt and R.R. Hake, Superconductivity at High Magnetic Fields, Phys. Rev. 131, (1). 140 (1963).
5. G.J. Van Gurp and D.J. Van Oijen, The Influence of Dislocations on Superconductivity, J. de Physique (1966), p. c-3-51.
6. R.J. Duffy and H. Meissner, Critical Temperatures and Critical Fields of Multiple Superconducting and Normal Conducting Films, Phys. Rev. 147, (1), 248 (1966).
7. R.E. Glover, III, Properties of Superconducting Films.
8. Y.B. Kim, C.F. Hempstead and A.R. Strand, Magnetization and Critical Currents, Phys. Rev. 129, (2), 528 (1963).
9. P.W. Anderson, and Y.B. Kim, Hard Superconductivity: Theory of the Motion of Abrikosov Flux Lines, Rev. Mod. Phys. 41 (1964).
10. J.D. Livingston, Defects and Magnetic Hysteresis in Type II Superconductors, Rev. Mod. Phys. Jan. 1964, p. 54.
11. T.H. Alden and J.D. Livingston, Magnetic Pinning in a Type II Superconductor Appl. Phys. Letters 8. (1) 6 (1966).
12. J.D. Livingston, Flux Pinning by Superconducting Precipitates, Appl. Phys. Letter 8 (12), 319 (1966).

13. R.D. Goolsby, Critical Temperature of Nb_3Sn in Various Microstructures, (M.S. Thesis), to be published.

14. T.G. Ellis, H.S. Whilhem, Phase Equilibria and Crystallography for the Niobium-Tin System, J. of the Less Common Metals, July 1964, p. 67-83.

15. R.E. Enstrom, Superconducting Properties of Nb_6Sn_5 and of Multi-phase Nb-Sn Alloys, J. Appl. Phys. 37. 13 (1966).

16. T.B. Reed, H.C. Gatos, W.J. LaFleur, and J.T. Roddy, Superconducting Behavior of Some β-Tungsten Structure Niobium Compounds and Their Alloys, In Metallurgy of Advanced Electronic Materials, G.E. Brock, Editor (Interscience Pub. Co., New York, 1963), Vol. 19, pg. 71.

17. R. Enstrom, T. Courtney, G. Pearsall, and J. Wulff, Current and Field Dependence of Superconductivity on Microstructures in the Nb-Sn System, in Metallurgy of Advanced Electronic Materials, G.E. Brock, Editor (Interscience Pub. Co., New York, 1963), Vol. 19 p. 12.

18. H.J. Fink and A.C. Thorsen, High Field Superconductivity of Carbides, Phys. Rev. 138. (4a) A1170 (1965).

19. B.D. Montgomery, Measurements on Niobium-Tin Samples in 200 kG Continuous Fields, Appl. Phys. Tetl. 6. (6) 108 (1965).

20. R.B. Flippen, Superconductive Transitions in Fast Pulsed Magnetic Fields, Phys. Rev. 137 6A (1965).

21. H.R. Hart, Jr., I.S. Jacobs, C.L. Kolbe, and P.E. Lawrence, Superconducting Critical Current of Nb_3Sn in Pulsed Magnetic Fields General Electric Research Lab Report No. 62-R1-2944 M, Jan. 1962.

22. F. J. Bachner and H. C. Gatos, Superconductivity Degradation in Beta Tungsten Structure Compounds - Nb_3Sn and Nb_3Al, Trans. Met. Soc. AIME 236 1262 (1966).

23. G. D. Cody and G. W. Cullen, Critical Currents and Lorentz-Force Model in Niobium Stannide, RCA Rev. Sept. 1964, p.466.

24. R. Hecht, Lower Critical Field of Niobium Stannide, RCA Review, Sept. 1964, p. 453.

ACKNOWLEDGMENTS

The author wishes to thank professors E. R. Parker and V.F. Zackay for their consultation and encouragement during the progress of this work. Also, many thanks to Mas Suenaga for his assistance with the experimental work. This work has been done under the auspices of the United States Atomic Energy Commission through the Inorganic Materials Reasearch Division of the Lawrence Radiation Laboratory.

Table I. Processing Treatments and Results

		Processing Treatment							
	Sample	Temp. T_1 (°C)	Time (min)	Pressure (psi)	Temp. T_2 (°C)	Time (min)	Pressure (psi)	H_{c_2} (kG)	T_c °K[a]
Sintered Type A	S2030S[b]	2030	8	8000	1100	15	8000		16.0
	S1950L	1950	8	8000	1100	60	8000	234	17.3
	S1930S	1930	8	8000	1100	15	8000	200	15.9
	S1900S	1900	8	8000	1100	15	8000	214	14.8
	S1840S	1840	8	8000	1100	15	8000		16.3
	S1730S	1730	8	8000	1100	15	8000	220	16.7
	S1730L	1730	8	8000	1100	60	8000	215	16.4
	S1600L	1600	8	8000	1100	60	8000		17.8
Sintered Type B	S1050	1050	30	1000	1880	8	1000	230	17.2
	S500	≈500	15	2000	1500	15	2000	215	17.8
Impregnated Type	IMP 1	≈800	15	1000	1050	2	1000	225	17.6

(a) T_c °K refers to the temperature at a median voltage.

(b) S is for the 15 min anneal and L is for the 60 min anneal.

Table II. Starting Materials

Material	Company	Mesh	Purity
Nb	Kawecki Chemical Co.	-325	99.9%
Sn	Cominco Elec. Natl.	-200	99.999%
C	Union Carbide Co.	(a)	< 2 ppm
Ta	Fansteel	-200 to -325	99.9%

(a) Spectroscopic Carbon

Table III. Current Densities and Resistivity Data

	Sample	J_{c_N} amp/cm^2 (a) (at 120kG)	J_{c_N} amp/cm^2 (b) (at 120kG)	ρ_n(μohm-cm) (c)	ρ_2(μohm-cm) (d)	%Nb_3Sn (e)
Sintered Type A	S2030S	-	-	-	7.5	3
	S1950L	1,030	12,900	69	2.4	8
	S1930S	1,610	53,700	40	6.1	3
	S1900S	980	-	112	-	-
	S1730S	1,020	3,520	111	0	29
	S1730L	800	6,660	120	2.9	12
	S1600L					19
Sintered Type B	S1050	3,000	27,200	24	0.5	11
	S500	1,700	11,300	48	-	15
Impregnated Type	IMP 1	3,400	-	4	-	-

(a) Current density of composite

(b) Current density of Nb_3Sn phase

(c) ρ_n: resistivity of normal sample at 4.2°k

(d) ρ_2: resistivity of sample at H=0 and 4.2°k

(e) Determined by lineal analysis of photomicrographs

Table IV. Phase Identification

	Sample	Phases Present					
		NbC (yellow)	Nb_2C (light brown)(c)	Nb_3Sn (dark blue or violet)	Nb_3Sn_2 (dark brown)(c)	Nb (light blue)	Sn (light yellow)
Sintered Type A	S2030S	x	-	x	x	-	x
	S1950L	x	x	x	x	-	x
	S1930S	x	-	x	x	-	x
	S1900S	x	x	x	x(a)	-	x
	S1730S	x	x	x	-	x	-
	S1730L	x	x	x	x	-	-
	S1600L	x	x	x	-	x	-
Sintered Type B	S1050	x	-	x	x(a)	-	x
	S500	x	-	x	x	x	-
Impregnated Type	IMP 1	-	-	x	x(b)	x	x

(a) red brown

(b) yellow brown - possibly Nb_2Sn_3

(c) No positive identification of composition

Table V. Sintering Temperature Versus % Nb_3Sn

Sample	% Nb_3Sn	Sintering Temperature °C
S2030S	3	2030
S1950L	8	1950
S1930S	3	1930
S1730L	12	1730
S1730S	29	1730
S1600L	19	1600

Table VI. Comparison of J_{c_N} and ρ_2 to % Nb_3Sn

	Sample	J_{c_N} (amp/cm^2)(a) @ 120 kG	J_{c_N} (amp/cm^2)(b) @ 120 kG	ρ_2(μohm-cm)	% Nb_3Sn
Sintered Type A	S2030S	-	-	7.5	3
	S1930S	1,610	53,700	6.1	3
	S1730L	800	6,600	2.9	12
	S1950L	1,030	12,900	2.4	8
	S1730S	1,020	3,520	0	29
	S1600L	-	-	-	19
Sintered Type B	S1050	3,000	27,200	0.5	11
	S500	1,700	11,300	-	15

(a) Current density of composite

(b) Current density of Nb_3Sn phase

Table VII. Comparison of Nb_3Sn Composition to H_{c_2} and T_c

Sample	Nb at.%	Sn at.%	H_{c_2} (kG)	T_c (°K)
S500	75.3	24.7	215	17.8
S1950L	75.7	24.3	234	17.3
S1730S	77.6	22.4	220	16.7
S1730L	78.4	21.6	215	16.4
S1050			230	17.2
S1930S			201	15.9

Table VIII. Comparison of Processing Treatment to J_{c_N} and ρ_n

	Sample	J_{c_N} (amp/cm^2)(a) (at 120kG)	J_{c_N} (amp/cm^2)(b) (at 120kG)	ρ_n (μohm-cm)	Tc (°k)	T_1 (°C)	Anneal Time (Min)
Sintered Type A	S1930S	1,610	53,700	40	15.9	1,930	15
	S1730S	1,020	3,520	111	16.7	1,730	15
	S1950L	1,030	12,900	69	17.3	1,930	60
	S1730L	800	6,600	120	16.4	1,730	60
	S1900S	980	-	112	-	1,900	15
Sintered Type B	S500	1,700	11,300	48	17.8	1,500(c)	0
	S1050	3,000	27,200	24	17.2	1,880(c)	0
Impregnated Type	IMP 1	3,400	-	4	17.6	1,035(c)	0

(a) Current density of composite

(b) Current density of Nb_3Sn phase

(c) T_2

Table IX. Critical Currents versus % Nb_3Sn

Sample	J_{c_N} (amp/cm^2)(a) (at 120kG)	% Nb_3Sn
S1930S	1,610	3%
S1730S	1,020	29%
S1950L	1,030	8%
S1730L	800	12%
S500	1,700	15%
S1050	3,000	11%

(a) Current density of composite

Table X. Physical Properties of Nb_3Sn

		Reference
T_c	15.9 - 17.8°K(median)[a]	
H_{c_2}	200 - 235 kG[a]	
a	5.282 - 5.290Å prepared at 1200°C	16
ρ	10 - 30 μohm-cm	24
ξ_o	88Å	25
λ	2900Å	25
d_c	380Å	
κ	34	24
H_o	2600 gauss	24
γ	1.5×10^{-2} cal/mole-deg	24
H_{c_1} (4.2°K)	188 G when T_c = 18°K $H_{c_1} = 200[1 - (T/T_c)^2]$	25

(a) Values from this work
(b) Obtained from Eq. 3 with λ = 2900 Å and κ = 34

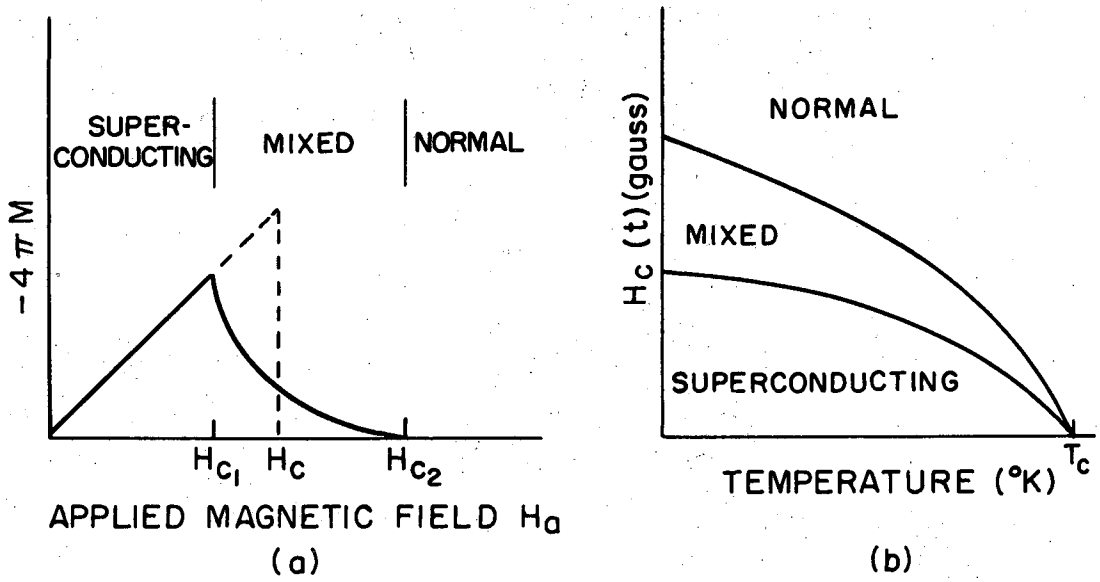

Fig. 1 a) Magnetization versus applied magnetic field for Type I and Type II Superconductors

b) $H_c(t)$ versus temperature with curves for $H_{c_1}(t)$ and $H_{c_2}(t)$.

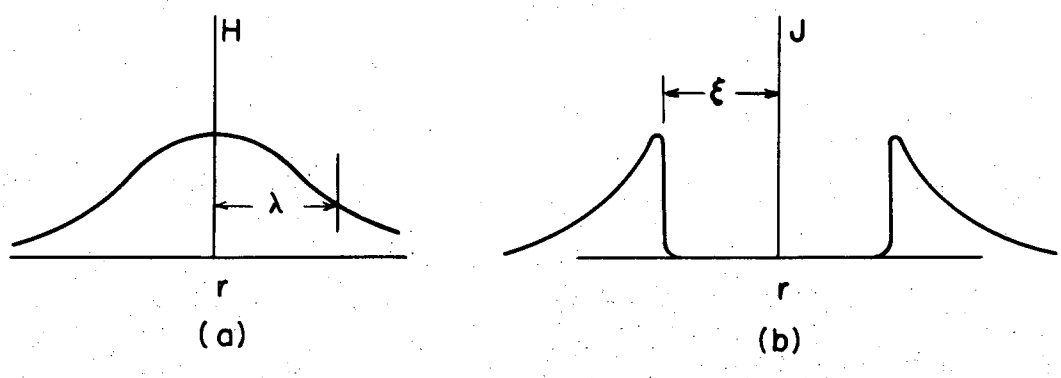

XBL 688-5788

Fig. 2 a) Decay of magnetic field near quantized flux line.

b) Current density in vicinity of quantized flux line.

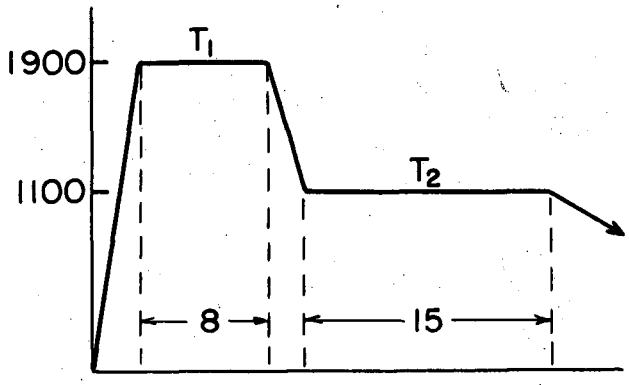

Fig. 3a Schematic of sintered Type A processing treatment.

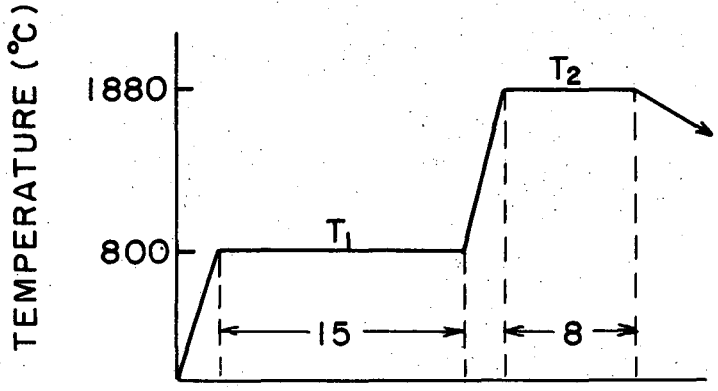

Fig. 3b Schematic of sintered Type B processing treatment.

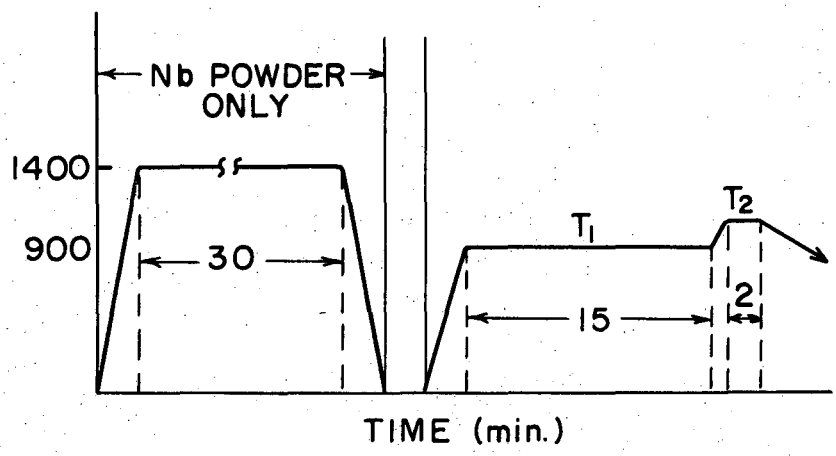

Fig. 3c Schematic of Impregnated Type processing treatment.

XBL 688-5790

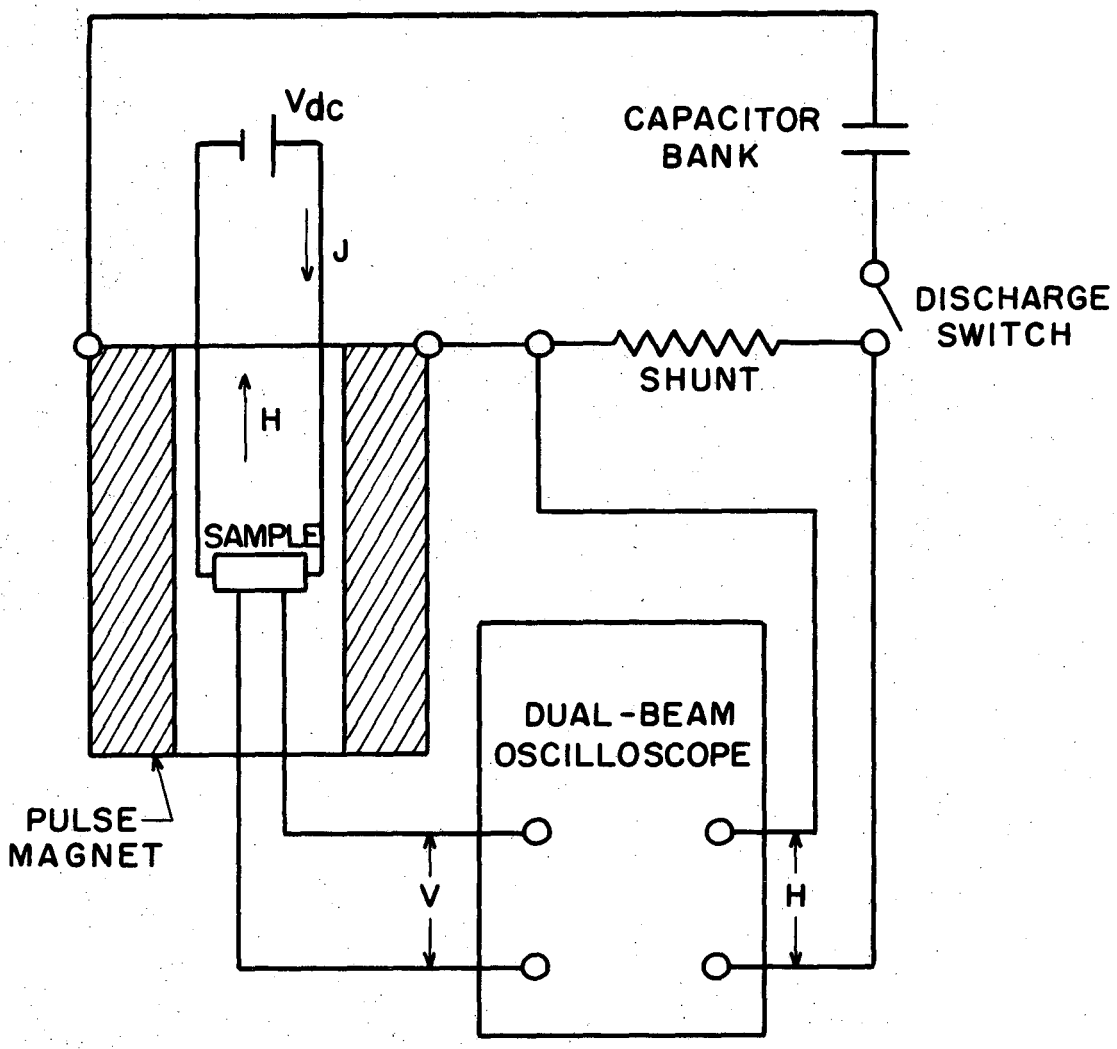

XBL 688-5787

Fig. 4 Schematic of pulsed field equipment.

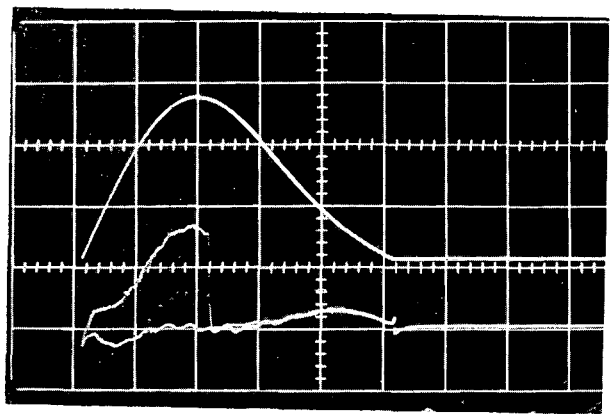

Fig. 5a Pulsed field record of sample S1950L.
Maximum H = 196 kG and J = 495 amp/cm^2.

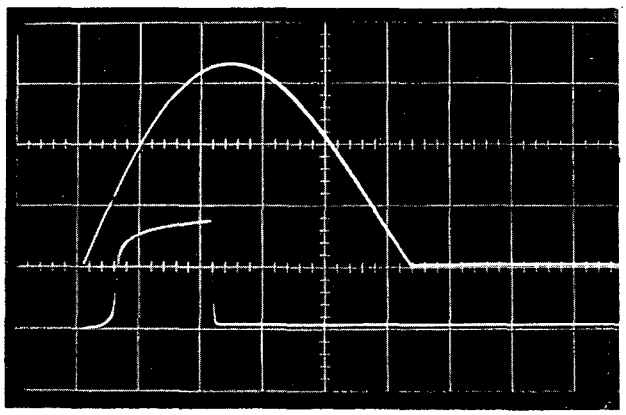

XBB 688-5111

Fig. 5b Pulsed field record of sample S1950L.
Maximum H = 26 kG and J = 3,240 amp/cm^2.

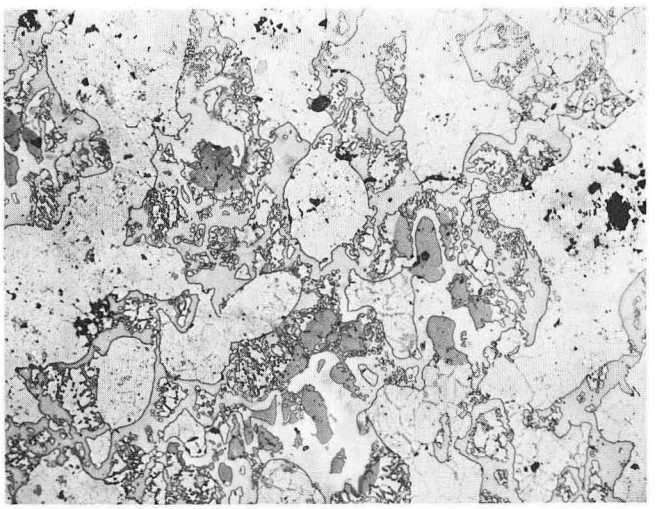

Fig. 6a Sample S1730S. Anodized. 250×

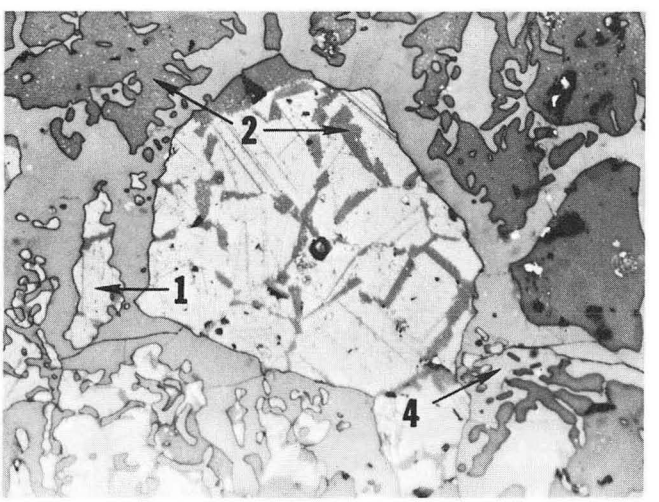

XBB 688-5054

Fig. 6b Sample S1730S. Anodized. 1000×
1-NbC 2-Nb_2C 4-Nb_3Sn

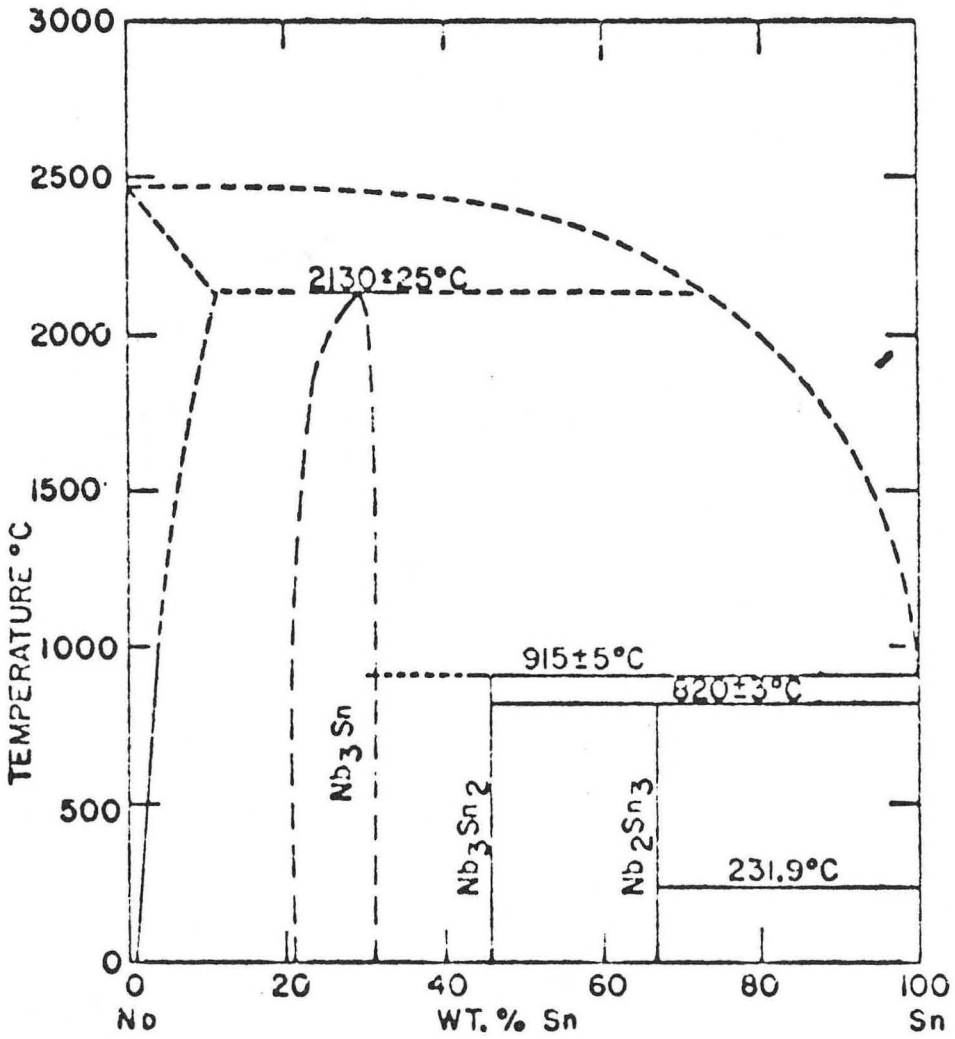

XBL 688-5700

Fig. 7 Niobium-Tin constitution diagram proposed by Ellis et al.[14]

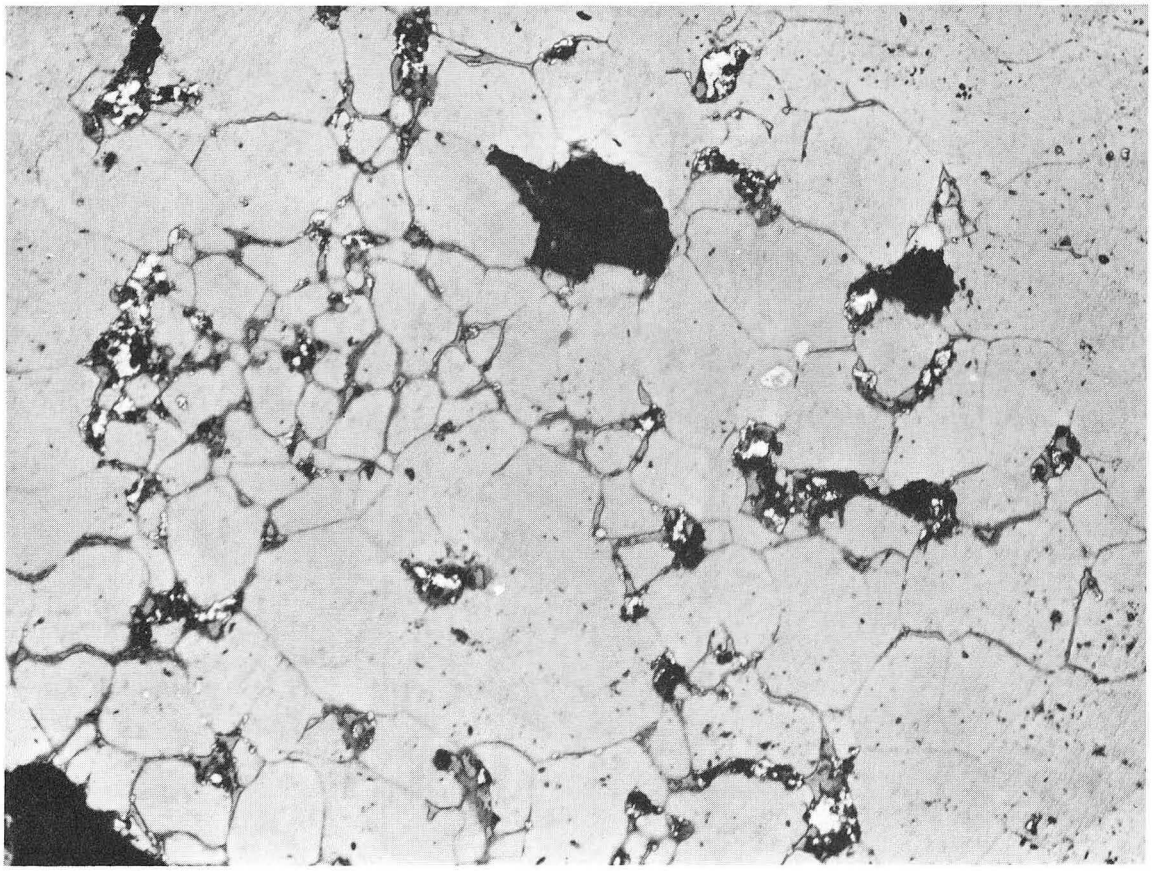

XBB 688-5051

Fig. 8 Sample S2030S. Anodized. 250×

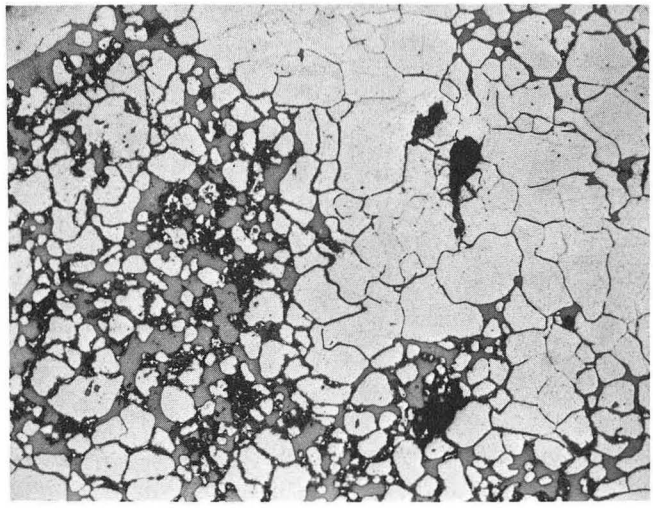

Fig. 9a Sample S1950L. Anodized. 250×

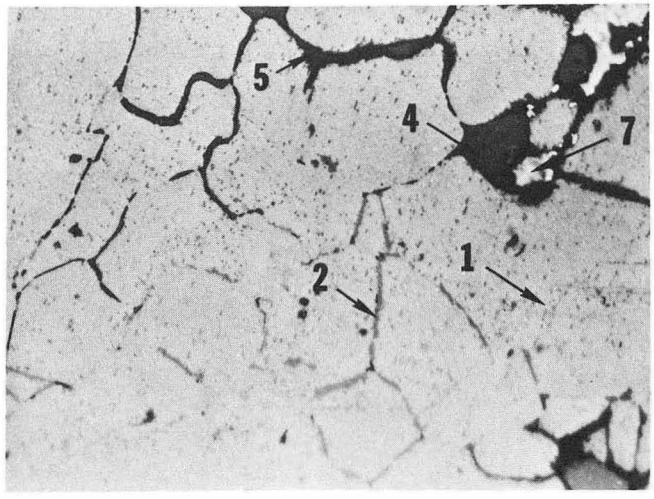

XBB 688-5061

Fig. 9b Sample S1950l. Anodized. 1000×

1-NbC 2-Nb_2C 4-Nb_3Sn 5-Nb_3Sn_2 7-Sn

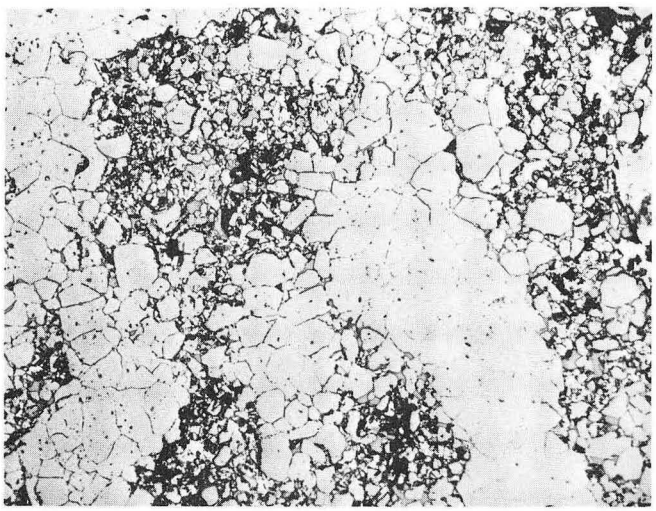

Fig. 10a Sample S1930S. Anodized. 250×

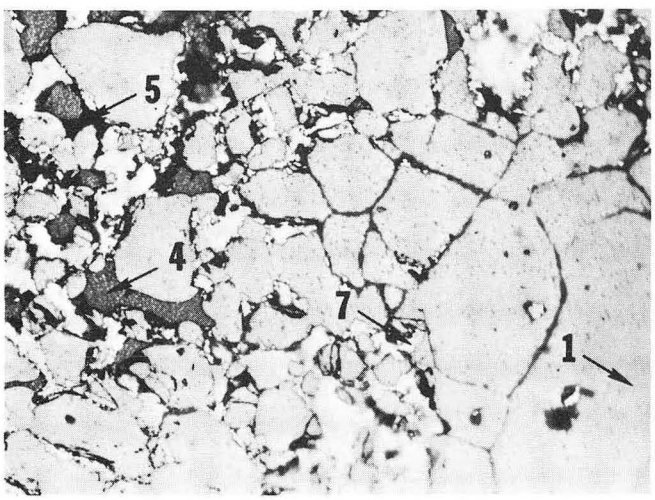

XBB 688-5053

Fig. 10b Sample S1930S. Anodized. 1000×
1-NbC 4-Nb_3Sn 5-Nb_3Sn_2 7-Sn

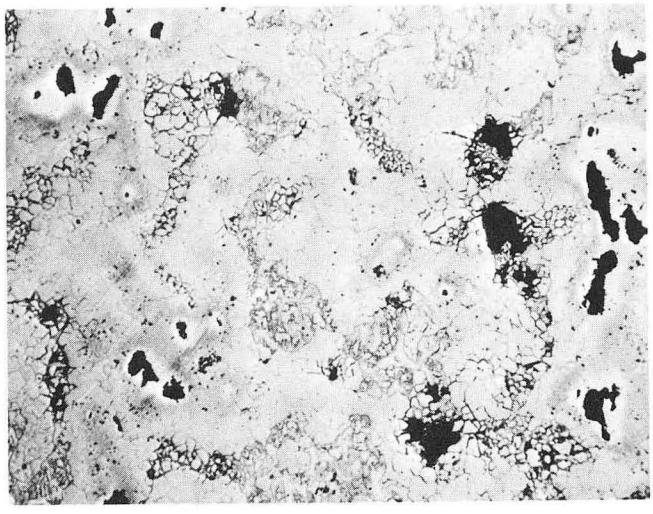

Fig. 11a Sample S1730L. Anodized. 100×

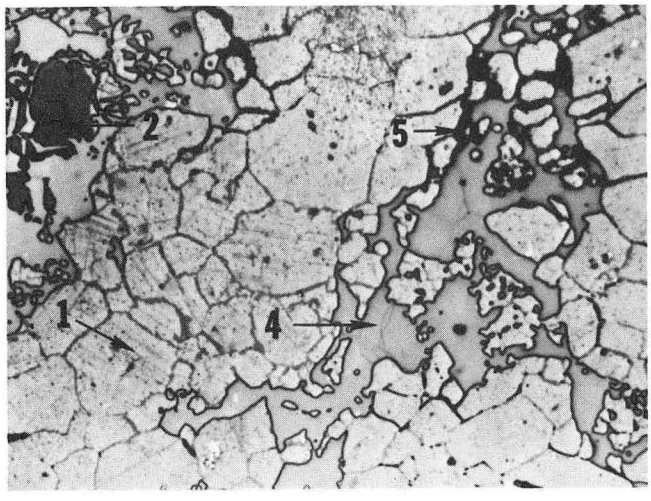

XBB 688-5055

Fig. 11b Sample S1730L. Anodized. 500×
1-NbC 2-Nb_2C 4-Nb_3Sn 5-Nb_3Sn_2

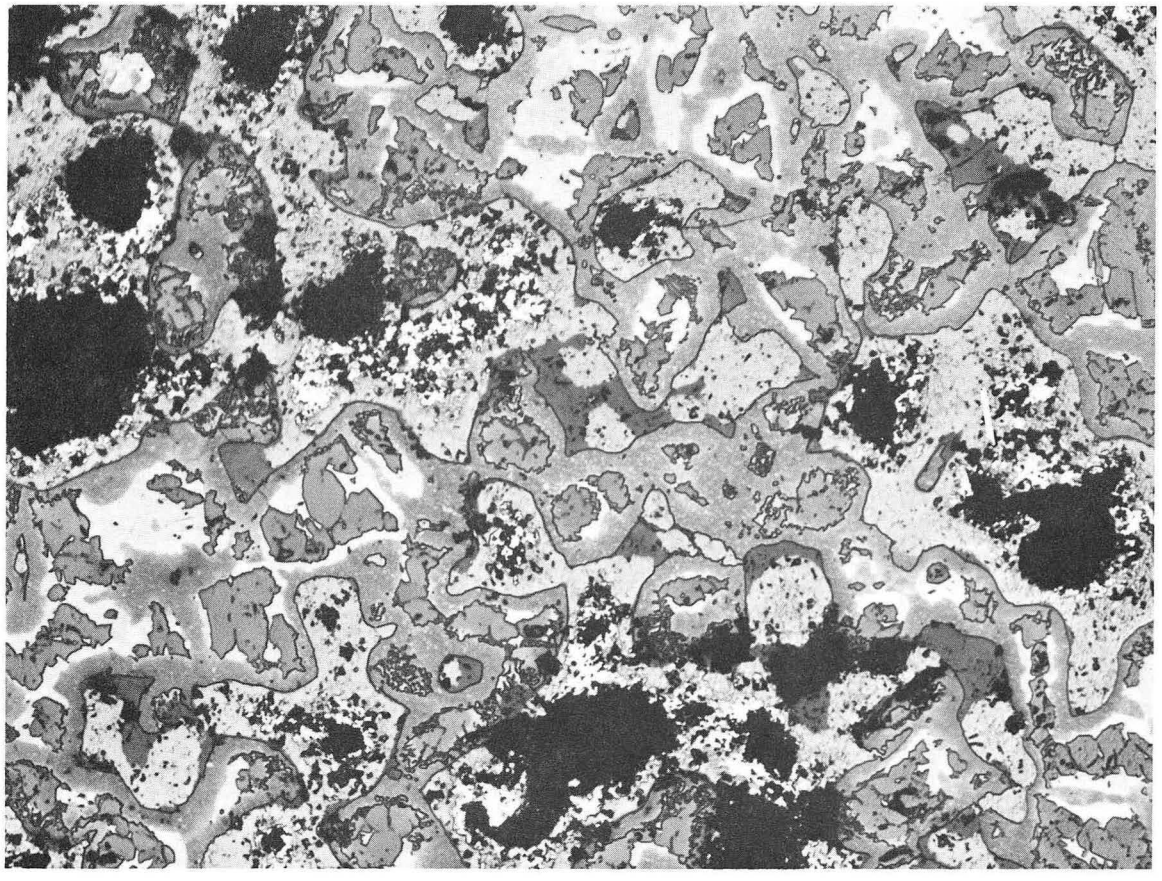

XBB 688-5057

Fig. 12 Sample S1600L. Anodized. 250×

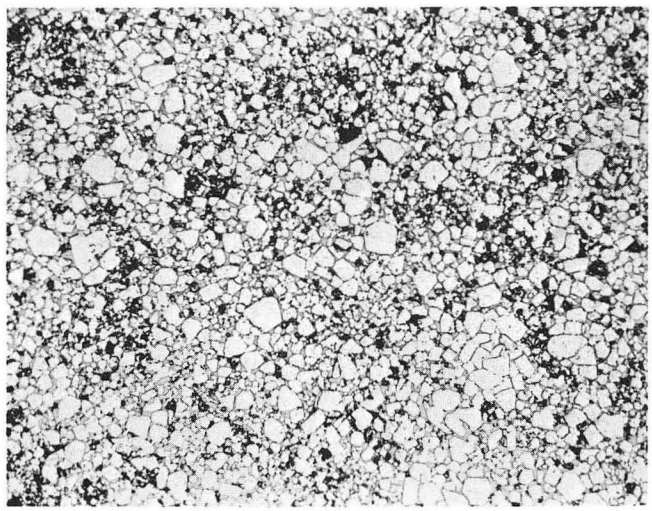

Fig. 13a Sample S1050. Anodized. 250×

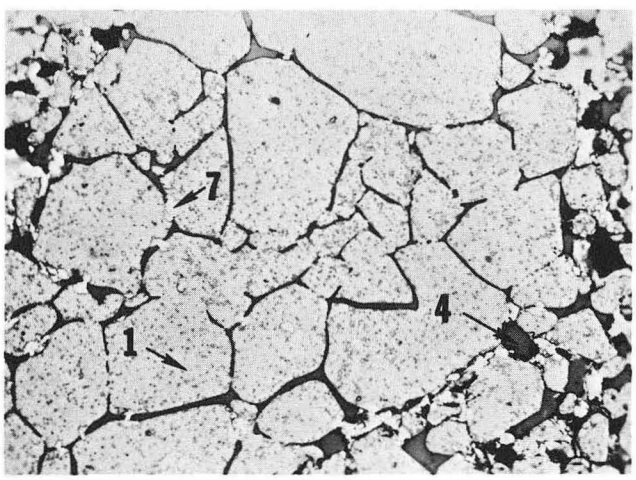

XBB 688-5058

Fig. 13b Sample S1050. Anodized. 1000×
1-NbC 4-Nb_3Sn 7-Sn

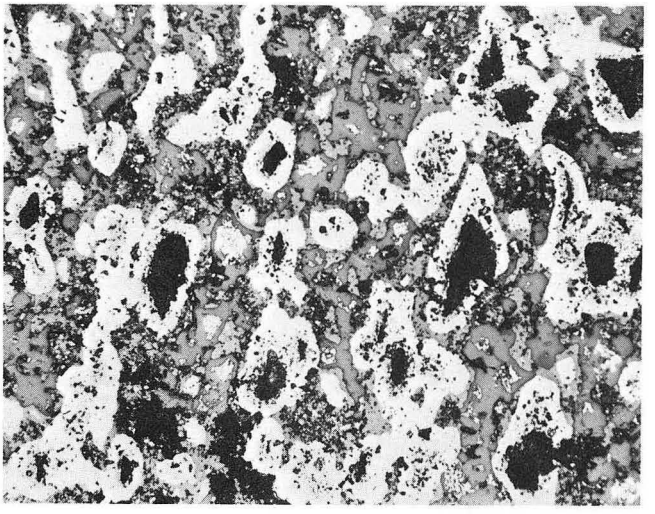

Fig. 14a Sample S500. Anodized. 250×

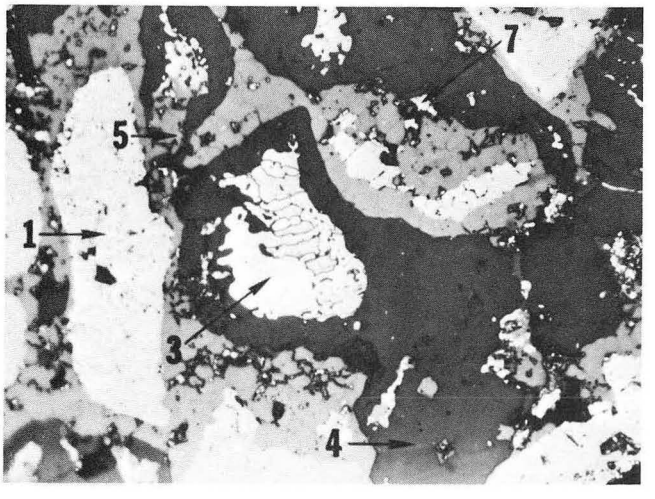

XBB 688-5059

Fig. 14b Sample S500. Anodized. 1000×
1-NbC 3-Nb 4-Nb_3Sn 5-Nb_3Sn_2 7-Sn

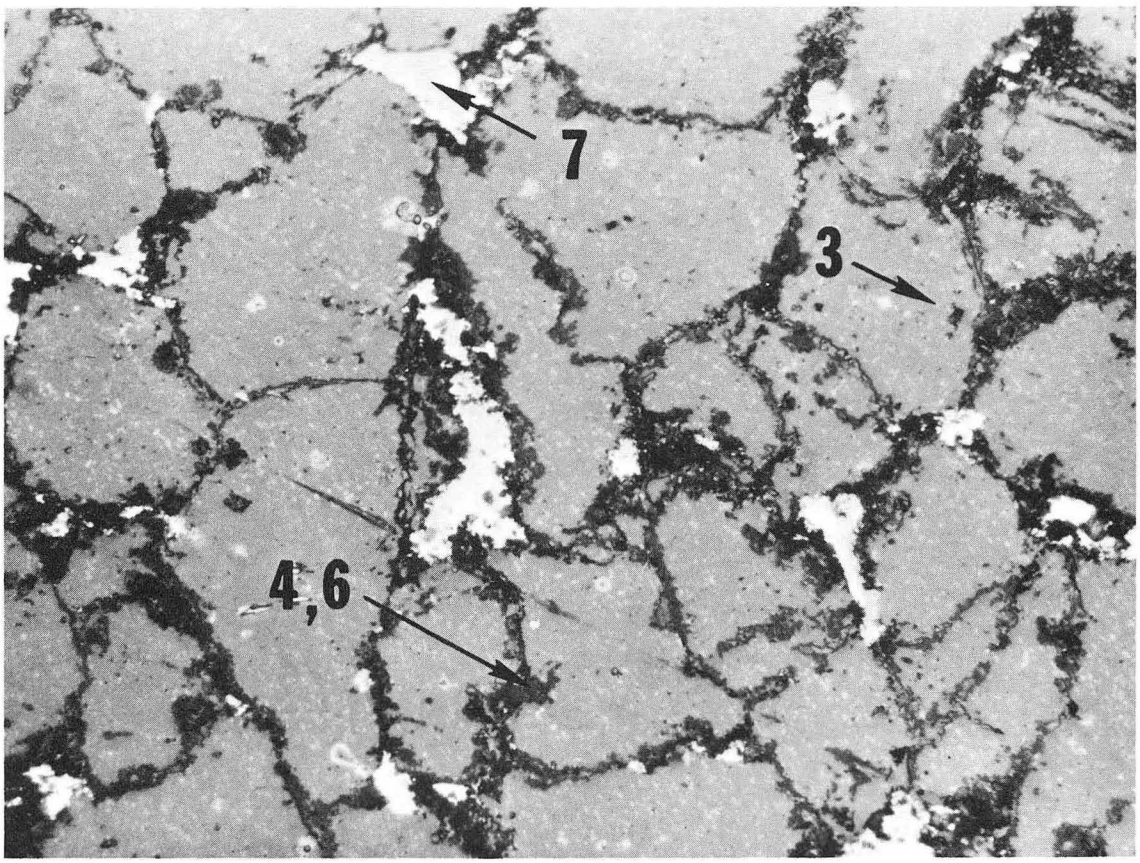

XBB 688-5060

Fig. 15 Sample IMP 1. Anodized. 500×
3-Nb 4-Nb_3Sn 6-Nb_2Sn_3 7-Sn

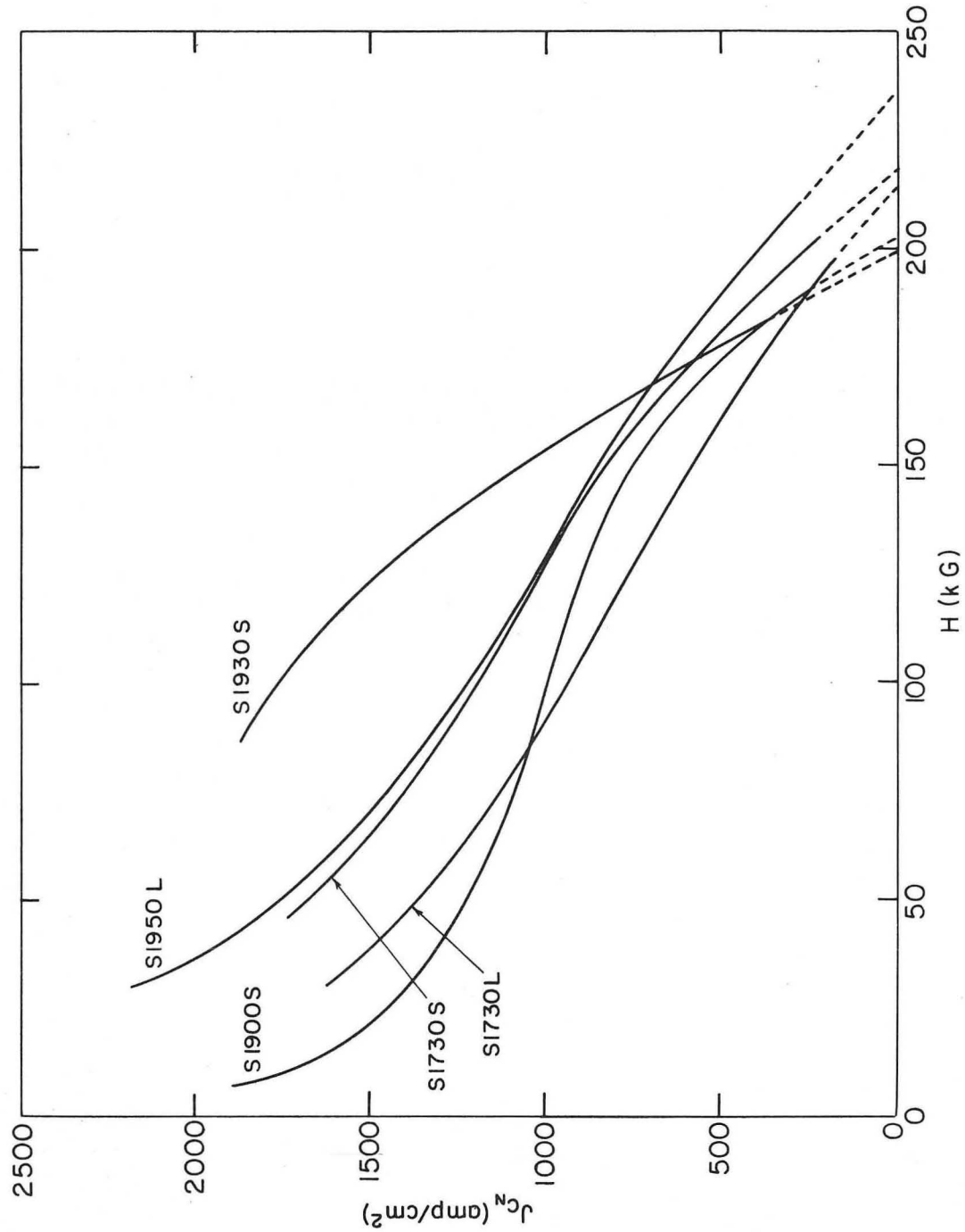

XBL 688-5794

Fig. 16 J_{c_N} versus H. Sintered Type A samples.

J_{c_N} is transition to normal state.

H is applied magnetic field. H $\perp$ J.

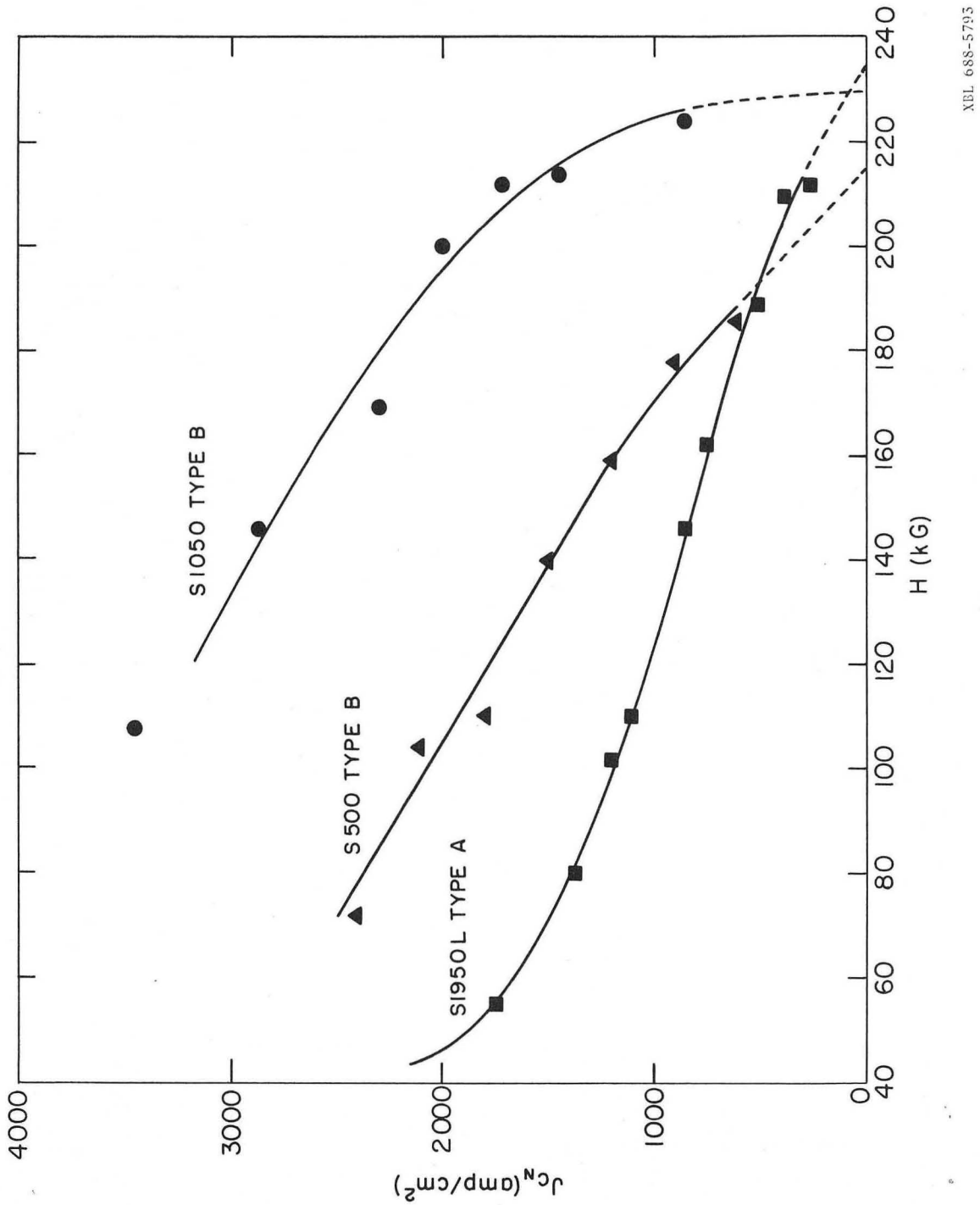

Fig. 17 J_{c_N} versus H. Sintered Type A and Type B samples. J_{c_N} is transition to normal state. H is applied magnetic field. $H \perp J$.

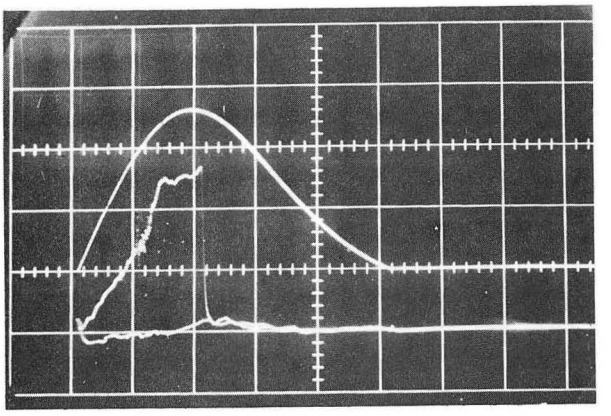

Fig. 18a Pulsed field record of sample S1730S.
Maximum H = 196 kG and J = 510 amp/cm^2
ρ_2 = 0

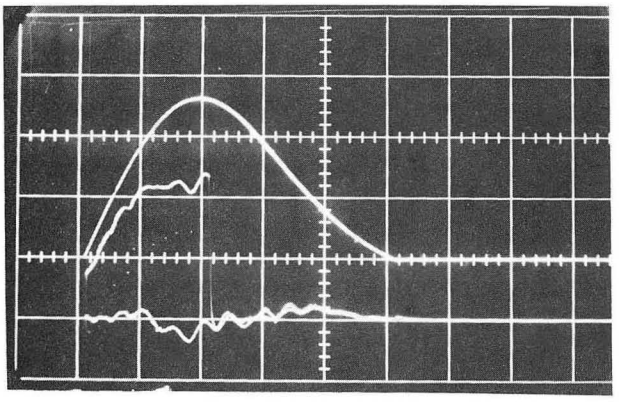

XBB 688-5112

Fig. 18b Pulsed field record of sample S1930S.
Maximum H = 196 kG and J = 695 amp/cm^2.
ρ_2 = 0.42 μohm-cm

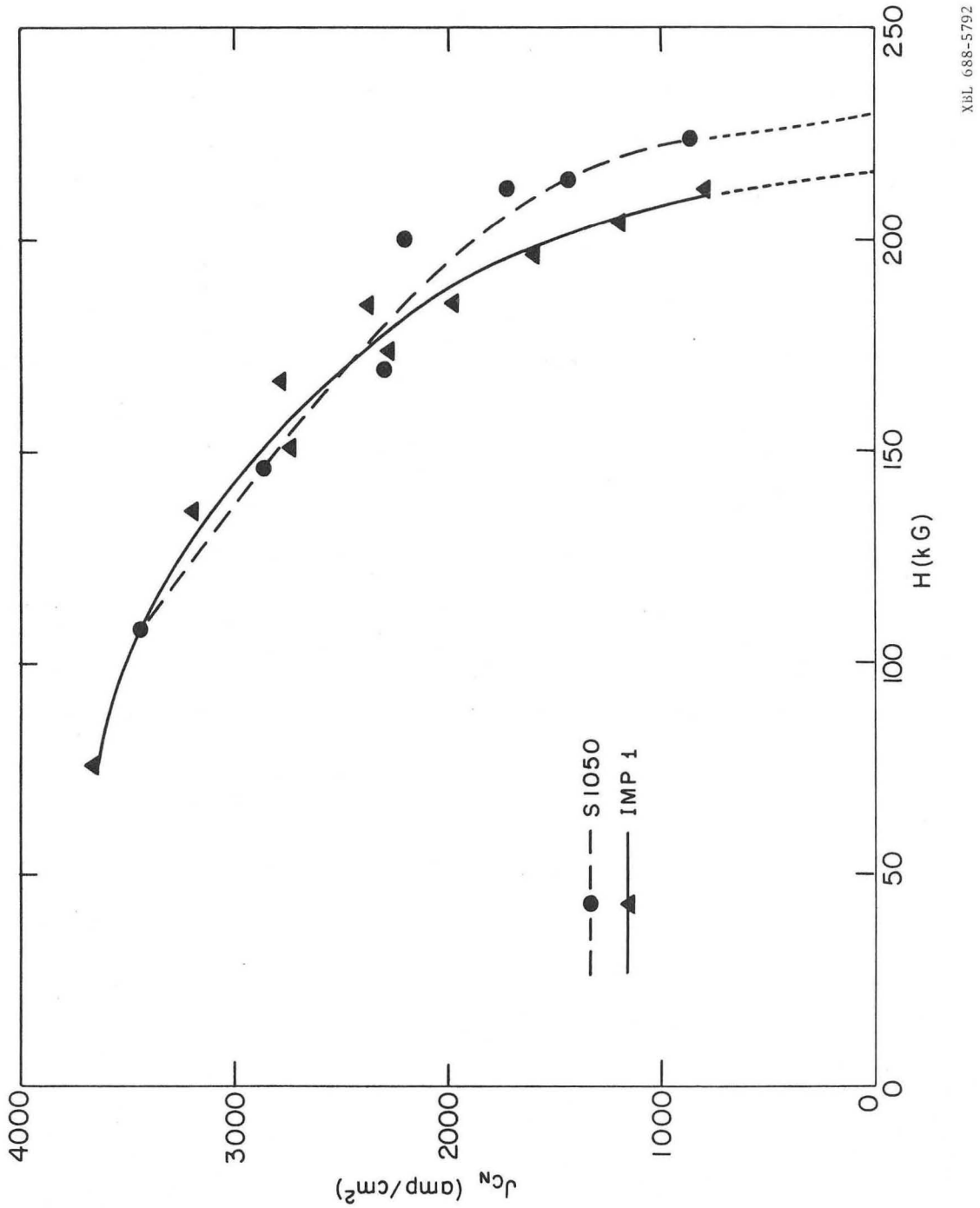

Fig. 19 J_{c_N} versus H. Comparison of sintered Type B to Impregnated Type. J_{c_N} is transition to normal state. H is applied magnetic field. $H \perp J$.

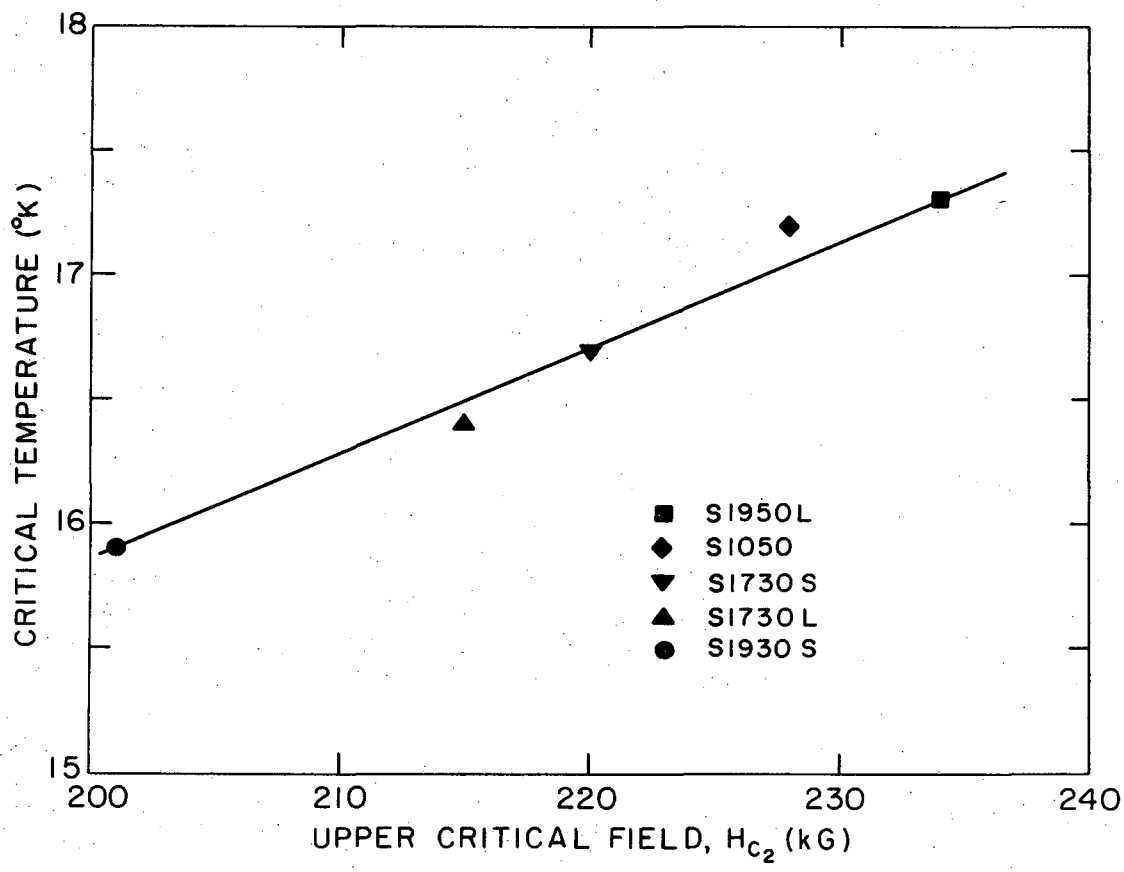

XBL 688-5785

Fig. 20 H_{c_2} versus T_c. Slope = $\rho_n \gamma$ assuming $H_{c_2} \propto \rho_n \gamma T_c$.